

Classical-trajectory time-dependent mean-field theory for ion-molecule collision problems

Alba Jorge*

*Departamento de Química, Universidad Autónoma de Madrid,
Cantoblanco, E-28049 Madrid, Spain*

Marko Horbatsch[†] and Tom Kirchner[‡]

*Department of Physics and Astronomy,
York University, Toronto, Ontario, Canada M3J 1P3*

(Dated: November 8, 2022)

Abstract

A mean-field model to describe electron transfer processes in ion-molecule collisions at the $\hbar = 0$ level is presented and applied to collisions involving water and ammonia molecules. Multicenter model potentials account for the molecular structure and geometry. They include charge screening parameters which in the most advanced version of the model depend on the instantaneous degree of ionization so that dynamical screening effects are taken into account. The work is implemented using the classical-trajectory Monte Carlo method, i.e., Hamilton's equations are solved for classical statistical ensembles that represent the initially populated orbitals. The time-evolved trajectories are sorted into ionizing and electron capture events, and a multinomial analysis of the ensuing single-particle probabilities is employed to calculate differential and total cross sections for processes that involve single- and multiple-electron transitions. Comparison is made with experimental data and some previously reported calculations to shed light on the capabilities and limitations of the approach.

* albamaria.jorge@gmail.com

† marko@yorku.ca

‡ tomk@yorku.ca

I. INTRODUCTION

Atoms and molecules are objects of the microscopic world. Hence, it seems natural to use quantum mechanics to describe their structure and interactions. What is natural is however not necessarily easy and perhaps not strictly required, at least as long as typical actions are much larger than Planck's constant. Put in more quantitative terms, in the $\hbar \rightarrow 0$ limit the quantum-mechanical Schrödinger equation can be replaced by classical equations of motion, which are easier to solve, and the time evolution of the quantum system be understood at the level of classical statistical mechanics [1].

In the context of atomic collisions this insight forms the basis of the classical-trajectory Monte Carlo (CTMC) method. It was introduced a long time ago [2] and has since been used in many different variants for a multitude of scattering problems, starting from the prototypical one-electron proton-hydrogen system, carrying over to multicharged-ion many-electron-atom systems, and more recently also finding application in problems involving molecular targets. A very large number of studies have been carried out and in many cases provided the first (and sometimes the only) theoretical results capable of describing complex experimental data [3].

It is beyond the scope of this chapter to provide a comprehensive overview of all these works. Interested readers are referred to [4, 5] for reviews and lists of references to the original literature. Our objective is more modest and specific: We describe a recently proposed CTMC method that extends the standard approach by incorporating dynamical screening effects in the spirit of a time-dependent mean-field model, and show by way of a few illustrative examples what can be learned from it when it is applied to the problem of single and multiple electron removal in ion-molecule collisions. We study total and differential cross sections. Both are needed for an accurate understanding of, e.g., the problem of radiation damage of biological tissue, which has been a major driver of contemporary ion-molecule collision studies. Differential data for electron emission provide more detailed information than total ionization cross sections but are harder to calculate on the basis of quantum-mechanical methods, especially those which do not make use of perturbative arguments. This makes CTMC calculations all the more important and motivated us to pursue this work.

Ion-molecule collision systems are many-particle problems. We address them in the frameworks of the semiclassical impact parameter approximation and the independent

electron model (IEM), which also form the basis of most quantum-mechanical approaches to the problem at hand. For us this means that the $\hbar \rightarrow 0$ limit is applied to a one-electron time-dependent Schrödinger equation whose Hamiltonian includes a mean-field potential to account for the electron-electron interactions in an effective manner and which has to be solved for the molecular orbitals (MOs) which form the molecular ground state, i.e., the initial state of the target before it is approached by the projectile ion.

The mean-field potential model used has a multicenter structure reflecting the molecular geometry and takes time-dependent screening effects into account. Our published work focuses on ion collisions with water (H_2O) molecules [6–9], which are of paramount interest for the radiation damage problem mentioned above, but more recently we have also looked at the proton-ammonia (NH_3) system [10], and we discuss it alongside the ion-water problem in this chapter.

The layout is as follows. We begin in Sect. II with a short summary of the general theoretical assumptions and ideas on which our model description is built. This is followed by somewhat more detailed discussions of the (time-dependent) mean-field potential models (in Sect. II A) and the procedures used to extract the desired information, i.e., collisional cross sections for various electron removal processes, from the solutions of the equations of motion (in Sect. II B). Results are presented and compared with experimental data and selected previous calculations in Sect. III, first for H_2O target molecules (in Sects. III A and III B) and then for NH_3 (in Sect. III C). The chapter ends with a few concluding remarks in Sect. IV. Atomic units, characterized by $\hbar = m_e = e = 4\pi\epsilon_0 = 1$, are used unless otherwise stated.

II. THEORY

We are concerned with relatively high-impact-energy ion-molecule collisions so that we can assume the projectile ion to travel on a straightline trajectory and the target molecule to remain rigid during the (short) interaction time. In other words, we use the semiclassical impact parameter approximation and freeze the rotational and vibrational degrees of freedom of the target. To deal with the many-electron nature of the problem we apply the IEM, i.e., we assume the Hamiltonian to be of single-particle form ($H \approx \sum_j h^{(j)}$) so that the equations of motion have one-electron character. Solving them for the MOs that form the molecular

ground state provides all accessible information on the electronic transitions taking place during the collision. The single-electron Hamiltonian has the standard form

$$h = \frac{\mathbf{p}^2}{2} + v_{\text{mod}} + v_{\text{p}}, \quad (1)$$

where v_{mod} denotes the multicenter target model potential and v_{p} the projectile potential. Both are specified in Sect. II A and together define the (time-dependent) mean-field model used.

Applying the $\hbar \rightarrow 0$ limit amounts in practice to solving Hamilton's equations for large sets of initial conditions which represent discretized versions of microcanonical ensembles of trajectories corresponding to the ionization energies of the MOs. For H_2O , a more detailed discussion of how the initial distributions are generated (along with plots to show them) is provided in [11]. An analogous procedure is used for NH_3 .

The trajectories are time evolved using a small step size of $\Delta t = 0.05$ a.u. until the projectile has reached a distance of about 500 a.u. to the target at the final time $t = t_f$ after passing it at a specific impact parameter vector. For each trajectory we look at the energy of the electron with respect to the projectile and the target in order to determine its fate: If one of them is negative the electron is considered bound to that center, i.e., it is either captured by the projectile or it remains bound to the target. If both energies are positive, the trajectory contributes to a transition to the continuum (ionization).

Calculations are carried out for many orientations of the target molecule characterized by randomly chosen sets of Euler angles, and orientation averages are calculated at the end in order to allow comparisons with orientation-insensitive experimental data. The models used to extract the differential and total cross sections for the processes of interest are described in Sect. II B.

A. Mean-field potential models

The ideas used to set up the (time-independent and time-dependent) mean-field potentials are the same for water and ammonia. Hence, we describe them for both target molecules in tandem.

1. Static screening model

The multicenter target (T) potentials are approximated as sums of (time-independent) central potentials for each atom of the molecule:

$$v_{\text{mod}} = \sum_i v_X(r_{X_i}) \quad (2)$$

$$= v_{\text{O}}(r_{\text{O}}) + \sum_{i=1}^2 v_{\text{H}}(r_{\text{H}_i}), \quad (T = \text{H}_2\text{O}), \quad (3)$$

$$= v_{\text{N}}(r_{\text{N}}) + \sum_{i=1}^3 v_{\text{H}}(r_{\text{H}_i}), \quad (T = \text{NH}_3). \quad (4)$$

In (2), X labels the atoms (X=O,N,H) and r_{X_i} are the distances from the active electron to the $i = 1, \dots, M$ nuclei of the molecule. Note that H_2O is planar while NH_3 is umbrella shaped. We use the following nuclear geometry parameters: The O-H bond lengths in H_2O are fixed at 1.8 a.u. and the angle between the position vectors for the two protons is 105° . The N-H bond lengths in NH_3 are 1.928 a.u., the azimuthal angles of the proton position vectors are 90° , 210° , and 330° and their polar angles are 108.9° [12]. A planar geometry would correspond to right polar angles. The central potentials in (2) are assumed to be of the form

$$v_X(r_X) = -\frac{Z_X - N_X}{r_X} - \frac{N_X}{r_X}(1 + \alpha_X r_X) \exp(-2\alpha_X r_X), \quad (5)$$

where $Z_X = 8, 7, 1$ are the nuclear charge numbers of X=O, N, H, while the other parameters have the values $N_{\text{O}} = 7.185$, $\alpha_{\text{O}} = 1.602$, $N_{\text{N}} = 6.2775$, $\alpha_{\text{N}} = 1.525$, $N_{\text{H}} = 0.9075$, and $\alpha_{\text{H}} = 0.6170$. These values were found as follows: At very large distances the total potential experienced by any one electron of a neutral atom or molecule behaves like $-1/r$. This condition results in the relations $N_{\text{O}} + 2N_{\text{H}} = 9 = N_{\text{N}} + 3N_{\text{H}}$. Using the first equality as a constraint, the parameters for H_2O were determined by minimizing the differences of the valence MOs' energy eigenvalues found for the (quantum-mechanical) Hamiltonian $\frac{\mathbf{p}^2}{2} + v_{\text{mod}}$ with respect to self-consistent field (SCF) results [11]. For NH_3 we use the same parameters N_{H} and α_{H} , find $N_{\text{N}} = 9 - 3N_{\text{H}} = 6.2775$, and determine the remaining parameter α_{N} such that the energy eigenvalues of $\frac{\mathbf{p}^2}{2} + v_{\text{mod}}$ are in reasonable agreement with the SCF results from [12].

If dynamical screening is excluded, the projectile potential of a fully-stripped ion is purely Coulombic: $V_{\text{p}} = -Z_{\text{p}}/r_{\text{p}}$ with Z_{p} and r_{p} being the charge number of the projectile and the

distance from it to the active electron. We treat the partially-stripped Si^{13+} ion for which we present results in Sect. III A in the same way, i.e., by a bare Coulomb potential corresponding to the asymptotic charge.

2. Dynamical screening model

Consider a small-impact-parameter collision of a highly-charged projectile ion. Around the distance of closest approach the projectile penetrates the molecule and exerts a strong force on the electrons. The likely outcome is *multiple* electron removal which increases the pull of the now partially ionized target on the electrons.

This dynamical effect can be modelled in a simple fashion by replacing the static screening charge parameters N_X in (5) by time-dependent ones in a way that ensures that the screening decreases with increasing degree of ionization q . The instantaneous degree of ionization corresponds to the (fractional) average number of removed electrons, the net electron removal $P_{\text{net}}^{\text{rem}}$. Hence, we can feed information on the degree of ionization into the potential by making the charge screening parameters dependent on $P_{\text{net}}^{\text{rem}}$. We use the simple ansatz

$$N_X(P_{\text{net}}^{\text{rem}}) = \begin{cases} N_X^c & P_{\text{net}}^{\text{rem}} \leq 1, \\ \frac{N_X^c N_T}{N_T - 1} \left(1 - \frac{P_{\text{net}}^{\text{rem}}}{N_T}\right) & 1 \leq P_{\text{net}}^{\text{rem}} \leq N_T, \end{cases} \quad (6)$$

where N_T is the total number of electrons in T (i.e., $N_T = 10$ for both H_2O and NH_3) and we have renamed the constant screening parameter of (5) by adding a superscript c . The idea of this model is that time-dependent screening¹ should not affect single ionization but kick in only after the $q = 1$ threshold has been overcome. It then changes linearly with the degree of ionization until all N_T target electrons are removed, at which point $N_X(P_{\text{net}}^{\text{rem}} = N_T) = 0$ for all X and the total potential reduces to a pure multicenter Coulomb potential [cf. (5) and (2)]. The model is similar in spirit to the *atomic* dynamical screening model proposed in [13]. We explain in Sect. II B 2 how $P_{\text{net}}^{\text{rem}}$, the only time-dependent ingredient, is calculated in the present CTMC-IEM approach.

One can take the dynamical screening model to the next level by also including time-dependent charge screening effects on the projectile ion. Here the rationale is that the screening of the projectile nucleus increases with an increasing number of captured electrons

¹ We use the terms time-dependent screening and dynamical screening interchangeably in this chapter.

and hence the strength of the projectile potential should be down-regulated accordingly. This can be accomplished by similar modelling as described above with the (fractional) net electron capture $P_{\text{net}}^{\text{cap}}$ taking the role of $P_{\text{net}}^{\text{rem}}$. We have reported on the implementation of such a model in [7]. For the collision systems studied, the effects of dynamical projectile screening were found to be relatively small compared to those of the dynamical target screening, except in situations in which capture into multiply-charged ions is the dominating electron removal process (see Sect. III B). We skip the technical details here and refer the interested reader to [7].

B. Analysis of electron capture and ionization processes

The ingredients of an IEM-based final-state analysis are single-particle probabilities for the processes of interest and multinomial statistics to combine them. We are interested in electron capture (cap) and ionization (ion) and in the latter case in total and differential probabilities and cross sections. The total probabilities for the j th MO ($j = 1, \dots, m$) are calculated as the ratios of the number of trajectories contributing to process $i = \text{cap}$ or $i = \text{ion}$ to the total number of trajectories

$$p_j^i = \frac{n_j^i}{n_{j,\text{tot}}}. \quad (7)$$

The differential probabilities are calculated by binning the ionized electrons in small intervals with respect to emission energy ΔE_{el} and emission angle $\Delta\Omega_{\text{el}} = 2\pi[\cos(\theta_{\text{el}_{i+1}}) - \cos(\theta_{\text{el}_i})]$ [6]. To arrive at this equation we have exploited the cylindrical symmetry and integrated over the azimuthal angle. The polar angles θ_{el_i} and $\theta_{\text{el}_{i+1}}$ define the interval for a given θ_{el} : $\theta_{\text{el}_i} \leq \theta_{\text{el}} < \theta_{\text{el}_{i+1}}$. In extension of (7) the single-particle ionization probability associated with ΔE_{el} and $\Delta\Omega_{\text{el}}$ is

$$\frac{d^2 p_j^{\text{ion}}}{dE_{\text{el}} d\Omega_{\text{el}}} = \frac{n_j^{\text{ion}}}{n_{j,\text{tot}} \Delta E_{\text{el}} 2\pi [\cos(\theta_{\text{el}_{i+1}}) - \cos(\theta_{\text{el}_i})]}. \quad (8)$$

1. Differential q -fold ionization

A situation of interest is the detection of one electron at $\{\Delta E_{\text{el}}, \Delta\Omega_{\text{el}}\}$, while a total of q electrons are ionized in the same event. In the simplest case of $q = 1$ the multinomial

combination of single-particle probabilities yields

$$\frac{d^2 P_{q=1}^{\text{ion}}}{dE_{\text{el}} d\Omega_{\text{el}}} = 2 \sum_{j=1}^m \frac{d^2 p_j^{\text{ion}}}{dE_{\text{el}} d\Omega_{\text{el}}} (1 - p_j^{\text{ion}}) \prod_{k \neq j}^m (1 - p_k^{\text{ion}})^2. \quad (9)$$

One can read this expression as follows: The differential single-electron probability for ionization from the doubly-occupied j th MO (8) is multiplied by a non-ionization probability from the same MO and by a factor of two to account for the spin degeneracy and ensure that exactly one out of two electrons of that MO end up in the continuum. The resulting binomial probability is further multiplied by non-ionization probabilities from all other MOs and summed over j since the detected continuum electron can originate from any of the initially occupied MOs. For higher q , the expressions follow the same logic but become more complicated. The cases $q = 2$ and $q = 3$ are shown explicitly in [6]. It is useful to define a *net* probability as the weighted sum of the q -fold probabilities

$$\frac{d^2 P_{\text{net}}^{\text{ion}}}{dE_{\text{el}} d\Omega_{\text{el}}} = \sum_{q=1}^{N_T} q \frac{d^2 P_q^{\text{ion}}}{dE_{\text{el}} d\Omega_{\text{el}}}. \quad (10)$$

The net probability corresponds to a measurement in which one detects one electron at $\{\Delta E_{\text{el}}, \Delta \Omega_{\text{el}}\}$ but does not determine if and how many additional electrons are ionized in the same event. It can also be calculated directly from the differential single-particle probabilities

$$\frac{d^2 P_{\text{net}}^{\text{ion}}}{dE_{\text{el}} d\Omega_{\text{el}}} = 2 \sum_{j=1}^m \frac{d^2 p_j^{\text{ion}}}{dE_{\text{el}} d\Omega_{\text{el}}}, \quad (11)$$

which provides a useful consistency check.

2. Charge-state correlated and inclusive probabilities

The total probabilities (7) are calculated at each time step, concurrently with the ensembles of trajectories, using the energy criterion described above. At the final time $t = t_f$ they form the basis of the analysis of single and multiple ionization and capture events within the IEM. The most straightforward approach is standard multinomial statistics for all charge-state correlated channels in which a number of k electrons are captured and l electrons are ionized to the continuum. The corresponding transition probabilities P_{kl} (which are functions of the

impact parameter vector) can be written as

$$P_{kl} = \sum_{k_1, \dots, k_m=0}^{M_1, \dots, M_m} \sum_{l_1, \dots, l_m=0}^{M_1, \dots, M_m} \delta_{k, \sum_i k_i} \delta_{l, \sum_i l_i} \prod_{i=1}^m \binom{M_i}{k_i + l_i} \binom{k_i + l_i}{k_i} (p_i^{\text{cap}})^{k_i} (p_i^{\text{ion}})^{l_i} (1 - p_i^{\text{cap}} - p_i^{\text{ion}})^{M_i - k_i - l_i}, \quad (12)$$

where $\delta_{k, \alpha}$ is the Kronecker delta symbol and $M_1 = M_2 = \dots = M_m = 2$ refer to the number of electrons in each MO. One problem of this analysis is that the N_T target electrons are distributed over the regions of space purely statistically, regardless of whether the projectile can accommodate a given number of electrons or not. This problem is most prominent for proton projectiles ($Z_p = 1$), which can capture one or two electrons, but not more than that. In fact, double capture leading to the formation of a negatively-charged hydrogen ion is already an extremely rare process which is known to involve electron correlations and which cannot be described at the level of the IEM, i.e., the multinomial evaluation of P_{kl} fails for $k \geq 2$ in the case of proton projectiles. One can try to correct for this by combining the single-particle probabilities in alternative ways such that the unphysical capture channels are closed [7, 13, 14], but such approaches can be criticized for their ad hoc character and they may show deficiencies in some of the open channels as a consequence of re-distributing the total capture flux among the physically allowed k, l combinations. In other words, there is no easy fix to the problem of unphysical multiple capture in the IEM and we will not consider it further in this contribution.

The more inclusive k -fold capture probabilities P_k^{cap} are given as

$$P_k^{\text{cap}} = \sum_{i=0}^{N_T - k} P_{ki}, \quad (13)$$

and can be used to calculate the net capture $P_{\text{net}}^{\text{cap}}$

$$P_{\text{net}}^{\text{cap}} = \sum_{k=1}^{N_T} k P_k^{\text{cap}}. \quad (14)$$

This is the analogue of (10) for differential ionization. The analogue of (11) is

$$P_{\text{net}}^{\text{cap}} = 2 \sum_{j=1}^m p_j^{\text{cap}}, \quad (15)$$

and similar equations for the total l -fold and net ionization probabilities can be established as well. We use (15) and its ionization counterpart to calculate the time-dependent net

capture $P_{\text{net}}^{\text{cap}}$, net ionization $P_{\text{net}}^{\text{ion}}$, and net removal $P_{\text{net}}^{\text{rem}} = P_{\text{net}}^{\text{cap}} + P_{\text{net}}^{\text{ion}}$, which feed into the dynamical screening models described in Sect. II A 2.

As a final comment we note that within the semiclassical impact-parameter approximation differential and total cross sections are obtained by integrating the probabilities for the processes of interest over the impact parameter vector.

III. RESULTS AND DISCUSSION

In this section, we present a selection of the results obtained from the CTMC mean-field approach described above. Our goal is to provide the reader with an overview and a general idea of what has been and can be accomplished in this framework, and where gaps in our understanding remain. The results are taken from our original research papers [6–8, 10] to which we refer the reader for more detailed discussions.

A. Collisions with water molecules: differential cross sections

We begin with differential electron emission from water molecules impacted by highly-charged high-velocity projectile ions. A useful parameter for this discussion is the ratio of the projectile charge to the projectile speed $\eta = Z_p/v_p$ measured in atomic units. Low values of η correspond to weak perturbations associated with little ionization of the target molecule. Electron capture is even less likely and can be ignored in the situations studied in this subsection. With increasing η one finds an increasing net ionization cross section, a growing fraction of which is due to multiple ionization events. Accordingly, we can expect time-dependent screening effects to increase in importance with η . The four collision systems studied here comprise the range $0.47 \leq \eta \leq 1.03$. They are 4 MeV/amu C^{6+} ($\eta = 0.47$), 3.75 and 3.0 MeV/amu O^{8+} ($\eta = 0.65$ and 0.73), and 4 MeV/amu Si^{13+} ($\eta = 1.03$) projectiles and were studied experimentally in [15–17]. Along with the data, perturbative quantum-mechanical calculations were reported, and we compare our results with those as well. The latter comparison is interesting since the two approaches complement each other: Ours is based on the $\hbar \rightarrow 0$ limit of quantum mechanics and uses a three-center target potential; the approach of [15–17] uses the quantum-mechanical continuum distorted-wave with eikonal initial-state (CDW-EIS) approximation coupled with a model in which molecular

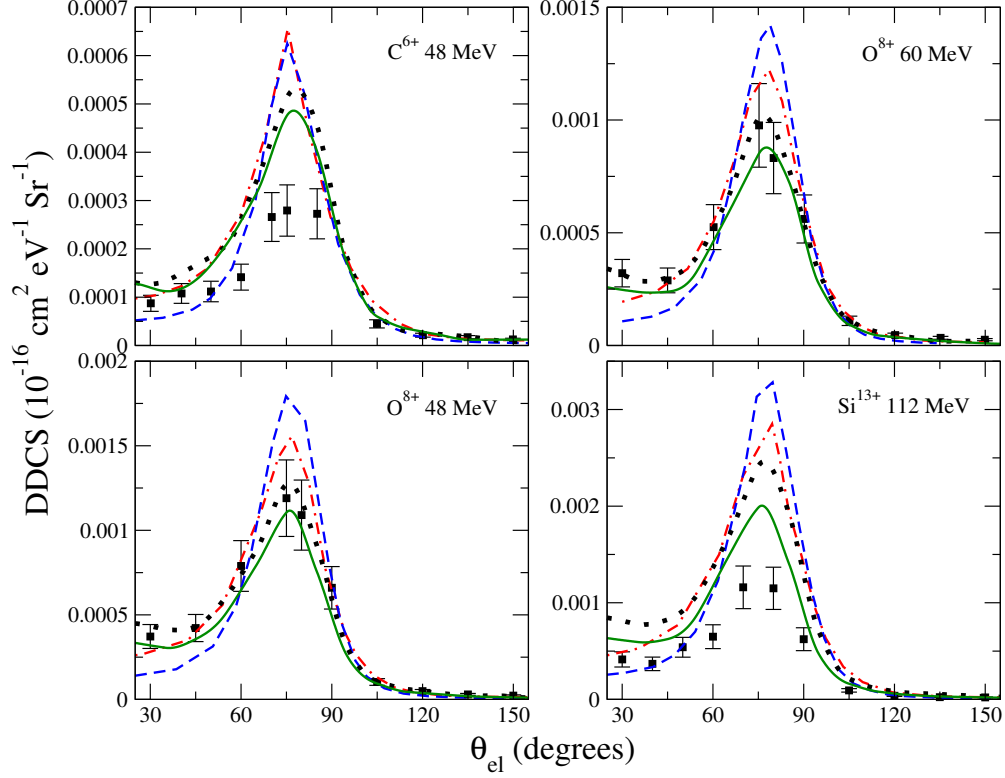


FIG. 1. DDCS for net ionization of water molecules as a function of electron emission angle in degrees, for the electron emission energy $E_{\text{el}} = 200$ eV. The CTMC results (obtained with angular resolution $\Delta\theta_{\text{el}} = 10^\circ$) are shown as dotted black (static screening) and solid green (dynamical screening) lines. The experimental data are shown as solid squares with error bars, and the prior and post CDW-EIS results are given by dashed-dotted red lines and dashed blue lines, respectively [15–17]. Adapted from [6]

cross sections are given as linear combinations of atomic contributions. Both work with single-electron Hamiltonians, i.e., are of IEM type.

In Fig. 1, doubly-differential cross sections (DDCSs) for net ionization are shown for the four collision systems. The electron emission energy is fixed at $E_{\text{el}} = 200$ eV and the DDCSs are shown as functions of the polar emission angle θ_{el} [cf. (8)]. As expected, there is an overall increase of the DDCS with η (note that the y -axis scales are different in the four panels). The time-dependent screening results are lower than those obtained with the static model potential, which is a reflection of the fact that the target potential becomes more attractive with decreasing charge screening parameters. At backward angles $\theta_{\text{el}} > 90^\circ$ the gap between both sets of results appears to widen with increasing η .

Truly quantum-mechanical effects are known to be the strongest at low and less important at higher electron emission energies, and indeed we find good overall agreement between the CTMC calculations and the experimental data at $E_{\text{el}} = 200$ eV. One may deem this energy value as medium given that it corresponds to a velocity of 3.8 a.u., to be contrasted with projectile speeds between 11.0 and 12.6 a.u. However, the level of agreement in the sequence of the four systems is not as expected: It is almost perfect for the O^{8+} projectiles, i.e., for the two intermediate η values, but the CTMC data appear to overestimate the measurements for the other two cases, C^{6+} and Si^{13+} impact at 4 MeV/amu, regardless of whether the static or time-dependent screening models are used. The overestimation appears to be independent of the emission angle, which might indicate that it is due to a problem with the overall normalization of the experimental data of [16].

Regarding the comparison with the CDW-EIS calculations, we note that two versions of the latter are shown, post and prior, which differ in the way the interaction between the ionized electron and the residual target ion is taken into account. In the post version, this interaction is purely Coulombic (using an effective charge), while in the prior form the influence of the non-ionized electrons on the dynamics of the continuum electron is included more explicitly. Hence, from a formal perspective the prior form is deemed superior [16].

As a general trend across all four systems we find the CTMC results at small (forward) angles to be slightly higher and in the peak region (around $\theta_{\text{el}} = 60 - 90^\circ$) lower than both CDW-EIS data sets, while there are no significant differences at backward angles. This gives the CTMC results a slight edge, since they match the angular shape of the experimental data very well in all cases. The CDW-EIS model for ion-atom collisions is known to be very good at accounting for two-center effects, i.e., the combined role of both the projectile and the residual target ion in shaping the angular distribution of medium-energy electrons [18, 19]. The present CTMC approach considers projectile and target interactions on the same footing as well, but in addition takes the three-center geometry of the target molecule fully into account. We are thus led to conclude that the angular distributions mirror a *many-center* electron-emission mechanism which only the present CTMC approach is able to describe properly.

The same conclusion can be drawn from Fig. 2, which displays singly-differential cross sections (SDCSs) as functions of the emission angle for the four collision systems. A closer analysis of the angular distributions in terms of a comparison of ratios of cross sections

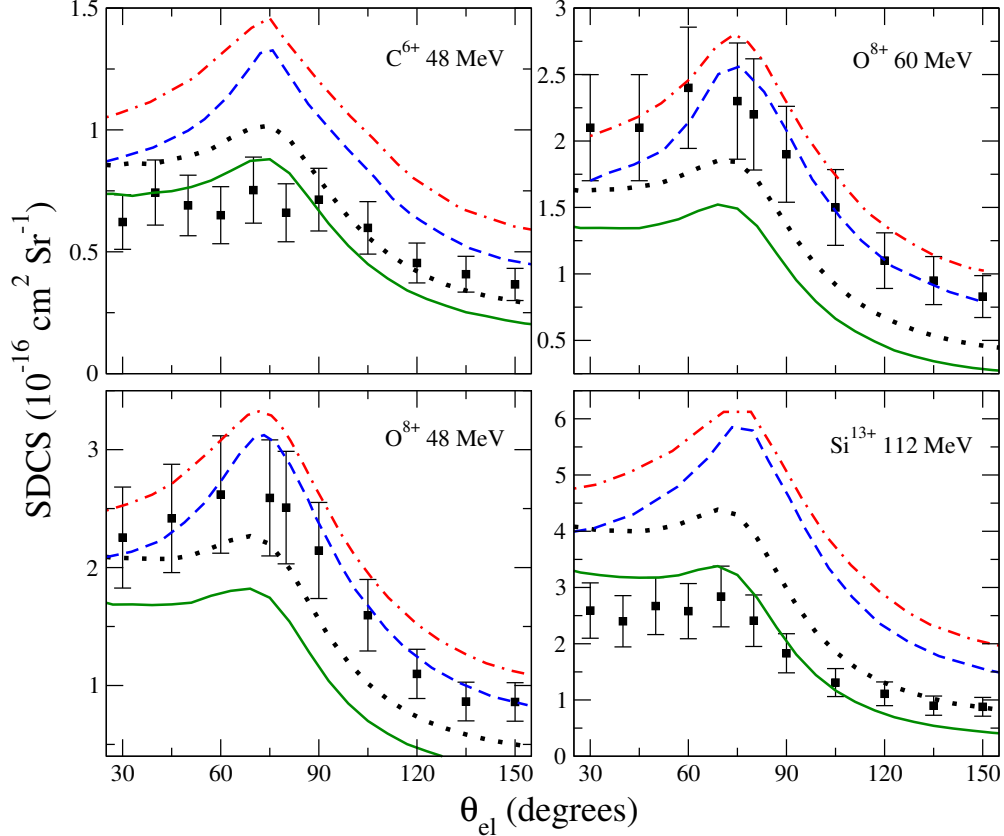


FIG. 2. SDCS for net ionization of water molecules as a function of electron emission angle in degrees, for the electron emission energy $E_{el} = 200$ eV. The CTMC results (obtained with angular resolution $\Delta\theta_{el} = 6^\circ$) are shown as dotted black (static screening) and solid green (dynamical screening) lines. The experimental data are shown as solid squares with error bars, and the prior and post CDW-EIS results are given by dash-dotted red lines and dashed blue lines, respectively [15–17]. Adapted from [6]

at forward vs intermediate scattering angles reveals that the CTMC results give a better representation of the experimental data than CDW-EIS, the prior version of which fares better than the post form, as expected [6].

On a quantitative level, there appears to be an inconsistency in the SDCSs of Fig. 2 and the DDCSs of Fig. 1 regarding the comparison between the CTMC and the experimental results: For the O^{8+} projectiles we found very good agreement for the DDCSs at $E_{el} = 200$ eV, but the SDCSs are underestimated. Likewise, for the other two projectiles the CTMC data appear to overestimate the measured DDCSs, but they are relatively close to the experimental SDCSs. These observations are, however, quite consistent, since the CTMC

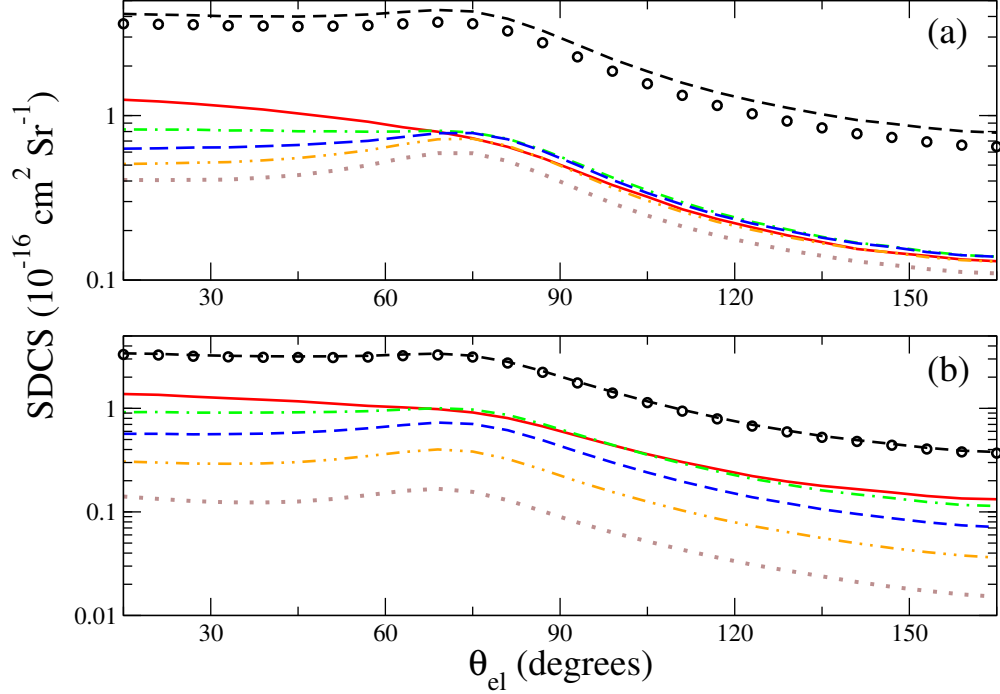


FIG. 3. SDCS for net ionization of water molecules as a function of electron emission angle in degrees for 112 MeV Si^{13+} projectiles with (a) static and (b) dynamical screening. (---) Net, (—) $\frac{d\sigma_1}{d\Omega_{\text{el}}}$, (-.-) $2\frac{d\sigma_2}{d\Omega_{\text{el}}}$, (-.-.-) $3\frac{d\sigma_3}{d\Omega_{\text{el}}}$, (-.-.-.-) $4\frac{d\sigma_4}{d\Omega_{\text{el}}}$, (-.-.-.-.-) $5\frac{d\sigma_5}{d\Omega_{\text{el}}}$, (o) $\sum_{q=1}^5 q\frac{d\sigma_q}{d\Omega_{\text{el}}}$. Adapted from [6]

approach is known to fall short for low-energy electron emission. Doubly-differential results at $E_{\text{el}} = 5$ eV, which are shown in [6], confirm this. In other words, an underestimation of the experimental SDCS is to be expected, and the fact that we do not observe it for C^{6+} and Si^{13+} projectiles points again to a possible overall normalization problem of the experimental data.

As for the static vs time-dependent screening model comparison we once again observe that the latter results in less ionization than the former and that this effect increases with η . In order to shed more light on the role of time-dependent screening we show in Fig. 3 for both CTMC models the contributions from the first five $q\frac{d\sigma_q}{d\Omega_{\text{el}}}$ terms to the net SDCS [cf. (10)] as well as their sum and the full net cross section for the Si^{13+} projectile for which η assumes the largest value among the four collision systems studied ($\eta = 1.03$).

For the σ_1 and $2\sigma_2$ terms the static and time-dependent screening results are similar, but higher-order contributions are suppressed in the time-dependent screening model and increasingly so with increasing electron multiplicity q . As a result, the sum truncated at

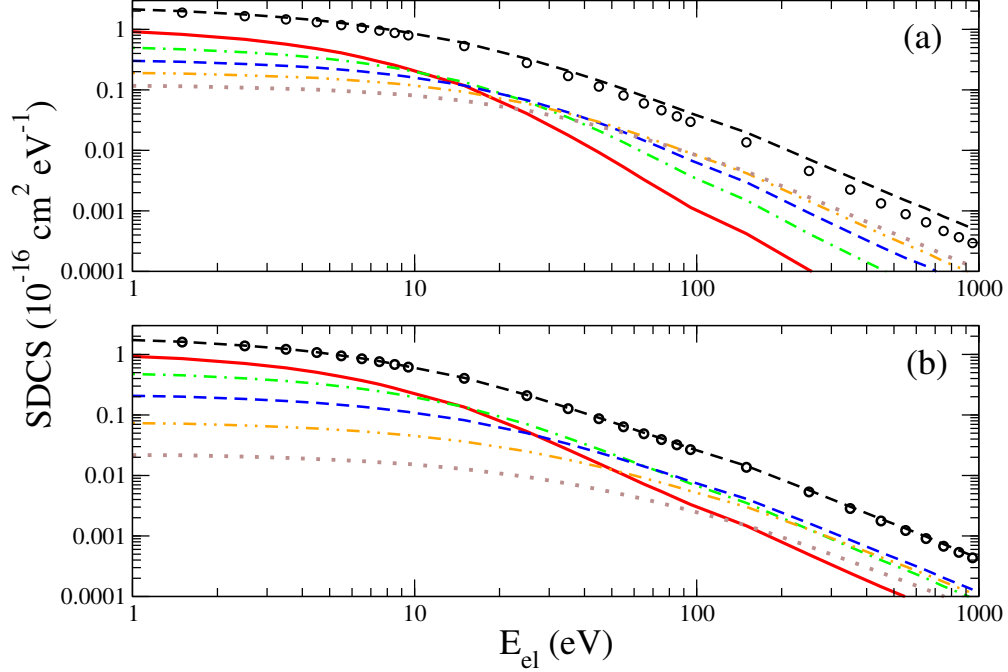


FIG. 4. SDCS for net ionization of water molecules as a function of electron emission energy for 112 MeV Si^{13+} projectiles with (a) static and (b) dynamical screening. (---) Net, (—) $\frac{d\sigma_1}{dE_{\text{el}}}$, (·-·-) $2 \frac{d\sigma_2}{dE_{\text{el}}}$, (- - -) $3 \frac{d\sigma_3}{dE_{\text{el}}}$, (· · - · ·) $4 \frac{d\sigma_4}{dE_{\text{el}}}$, (· · · ·) $5 \frac{d\sigma_5}{dE_{\text{el}}}$, (○) $\sum_{q=1}^5 q \frac{d\sigma_q}{dE_{\text{el}}}$. Adapted from [6]

$q = 5$ is very close to the full net cross section, i.e., contributions from $q > 5$ account for at most 3% in the time-dependent screening model. For the static case those contributions range between 13% at small emission angles and 18% at backward angles.

A complementary view is provided by a similar comparison of cross sections differential in electron emission energy instead of emission angle. Such a comparison is shown in Fig. 4. At low electron energies the contribution from the excluded $q > 5$ terms is very small in both screening models, but the situation is different at higher E_{el} . At the highest energies shown, the contribution from those high- q terms is almost as large as that from $q \leq 5$ in the case of the static model, whereas it stays below 10% if time-dependent screening is turned on. It would be of great interest if differential experimental data for fixed q would become available to test these predictions.

B. Collisions with water molecules: total cross sections

We now turn our attention to total cross sections for processes that involve the removal of one or several electrons. Figure 5 displays the pure ionization cross sections σ_{01} and σ_{02} calculated with the trinomial formula (12) for the $\text{Li}^{3+}\text{-H}_2\text{O}$ collision system. Three CTMC data sets are shown: static screening results, results obtained from using the time-dependent target charge screening parameters (6), and results from calculations in which time-dependent projectile screening effects are also included. Obviously, the three models give very similar results over the range of impact energies shown and they do not agree very well with the experimental data. The underestimation of σ_{01} can, once again, be explained by a known weakness of the CTMC approach, namely a shortfall at large impact parameters which dominate singly ionizing collisions. Since ionization at large impact parameters is mostly associated with low-energy electron emission, this is the same weakness as the one identified in Sect. III A above.

Figure 6 shows the net capture cross section for the same collision system. Only static screening ('CTMC static') and time-dependent target *and* projectile screening ('CTMC dynamic') results are included, but we note that the target-only time-dependent screening cross section is very close to the 'CTMC dynamic' data shown.

At high impact energies, the static and dynamic results are very similar — there simply is not enough time for the mean-field potential to adapt and thereby change the character of the trajectories. Below $E \approx 100$ keV/amu, however, time-dependent screening effects are strong, as can be seen most clearly in the inset which displays the cross section on a linear scale.

In addition to the CTMC results the figure includes experimental data from [20] and results from two sets of quantum-mechanical independent-atom-model (IAM) calculations: 'IAM-AR', in which the simple additivity rule is used to sum up atomic cross sections, and 'IAM-PCM', which is a much more sophisticated model which takes the geometric overlap of the atomic cross sections into account [21]. Interestingly, the static-potential CTMC results agree well with the IAM-AR data, while the time-dependent screening calculations are closer to the IAM-PCM cross sections. A similar pattern was observed for He^{2+} impact [8]. At $E \geq 200$ keV/amu the results from all four models merge and show good agreement with the experimental data. As discussed in [8], it is difficult to understand from a modelling

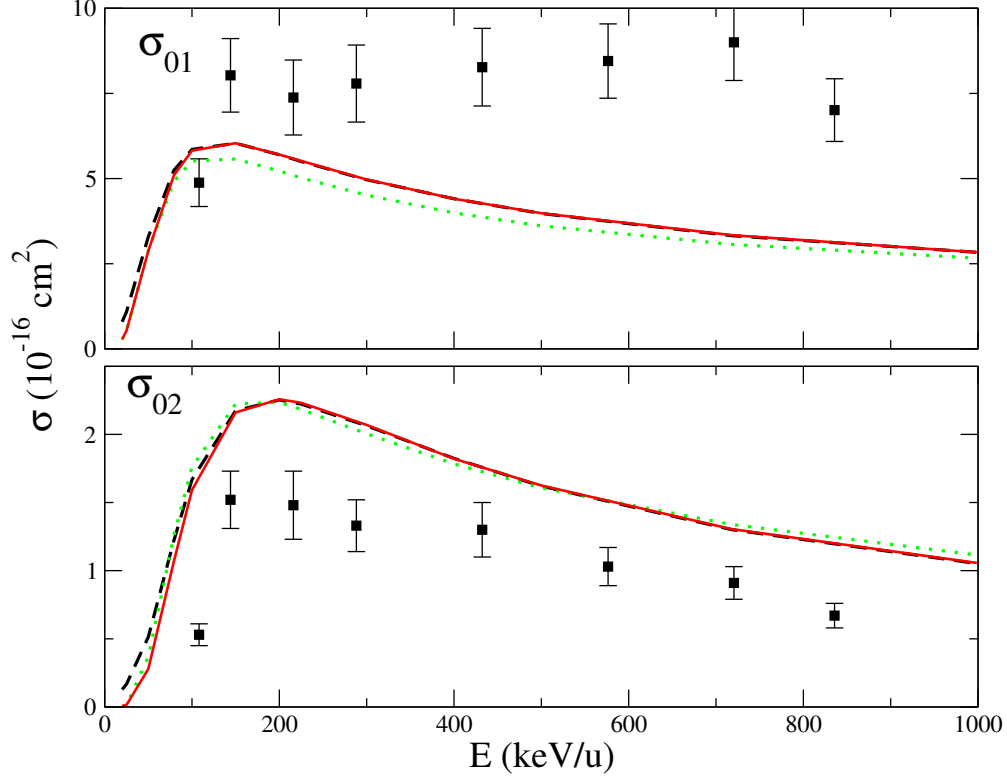


FIG. 5. Pure single and double ionization cross sections for Li^{3+} - H_2O collisions as functions of impact energy. The CTMC results are shown as dashed black (dynamical target and projectile screening), solid red (dynamical target screening), and dotted green (static screening) lines. The experimental data are shown as solid squares with error bars [20]. Adapted from [7]

perspective why all calculated cross section curves for Li^{3+} impact are significantly above the two experimental data points at $E < 200$ keV/amu. This observation is also in striking contrast to what was found for He^{2+} impact and warrants further investigation, ideally aided by additional experimental work.

We end this subsection with a comparison between static and dynamic screening model results which uses similar ideas as in Figs. 3 and 4, but this time on the basis of *total* cross sections: Figure 7 displays for four different projectiles (He^{2+} , Li^{3+} , C^{6+} , Ne^{10+}) the percentage contribution of $\sigma_a = \sum_{q=1}^3 q\sigma_q^{\text{rem}}$ to the total net removal cross section $\sigma_{\text{net}}^{\text{rem}}$ as a function of the parameter $\eta = Z_p/v_p$. A value of close to 100% signals that the $q \geq 4$ contributions to $\sigma_{\text{net}}^{\text{rem}}$ are negligibly small. This is the situation observed in the perturbative small- η regime. As η increases, all the curves in Fig. 7 show a decreasing trend, eventually reaching a first minimum located at an η value which is larger, the larger the projectile

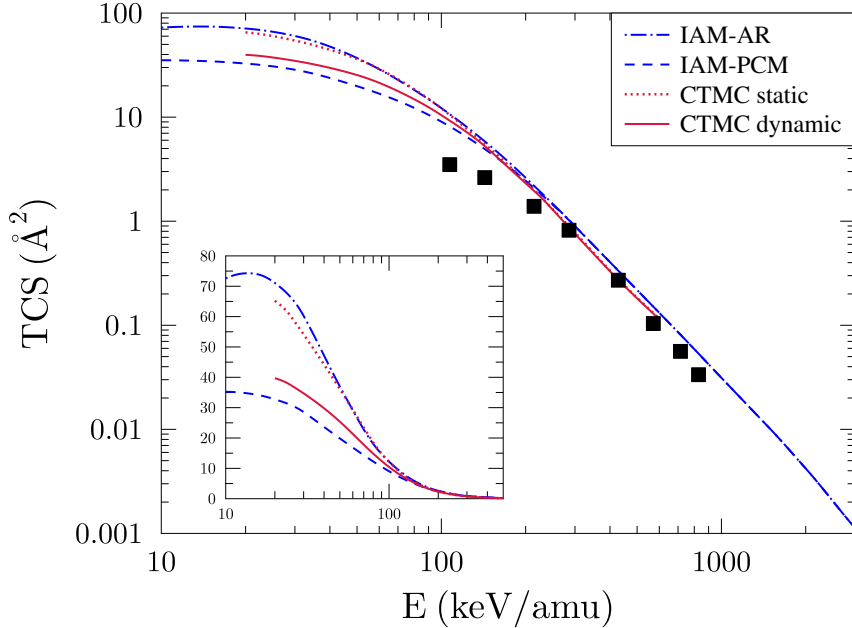


FIG. 6. Net electron capture cross section for Li^{3+} - H_2O collisions as a function of impact energy. The highest curve (dash-dotted blue) shows the additivity rule result (IAM-AR), the lowest (dashed blue) curve the IAM-PCM result. In between are the CTMC results, namely the (dotted red) static screening, and below it (solid red) the dynamical screening result. The experimental data are shown as black solid squares [20]. Adapted from [8]

charge is. The minimum is followed by a local maximum and then another decrease. A closer analysis of the data shows that for each projectile the minimum occurs in a region in which ionization is the dominant electron removal process. Capture becomes competitive around the maximum and takes over as the dominant process at even higher η values.

For the static screening results displayed in panel (a) the minima are deep, in particular for the highly-charged projectiles, indicating that high-multiplicity (i.e., $q > 3$ -fold) ionization is predicted to be very strong. Once time-dependent target screening is included [panel (b)], high- q processes are suppressed and the minima become shallower. Additional inclusion of time-dependent projectile screening [panel (c)] affects the data mostly at large η values, i.e., in the region in which capture becomes dominant.

There is no apparent scaling with respect to η : When moving from one projectile to the next, the positions of the minima and maxima change in nontrivial ways. This is perhaps not

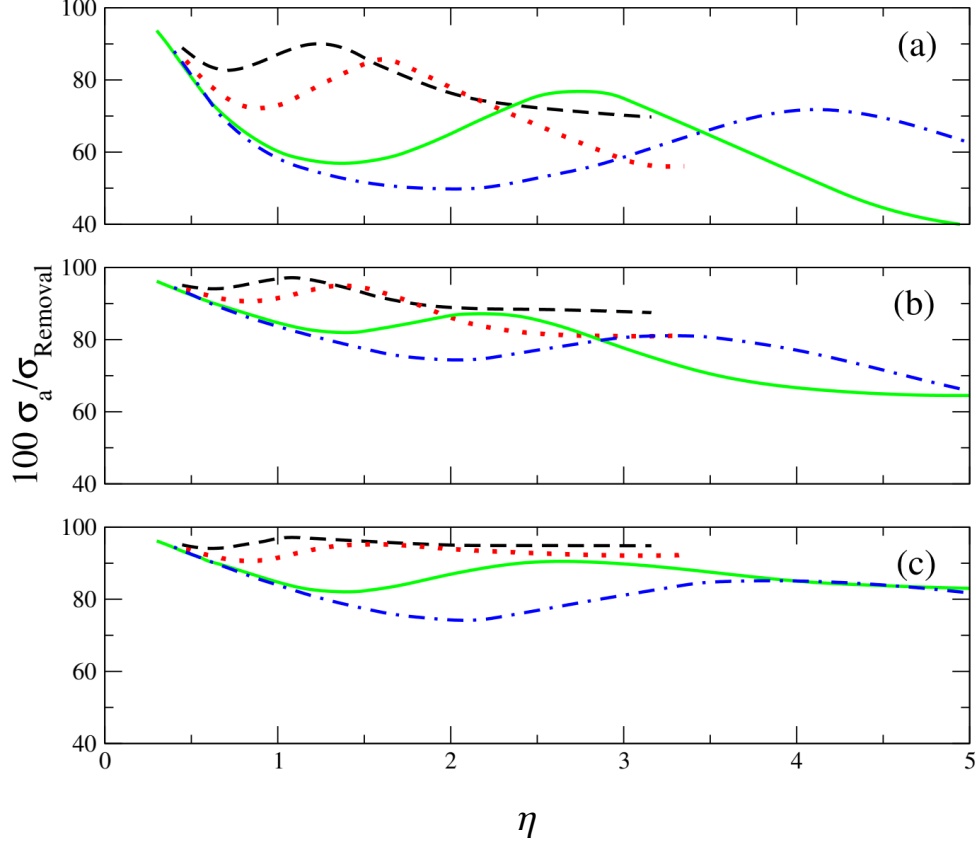


FIG. 7. Percentage of $\sum_{q=1}^3 q\sigma_q^{\text{rem}} = \sum_{q=1}^3 q(\sigma_q^{\text{cap}} + \sigma_q^{\text{ion}})$ with respect to the total net removal cross section $\sigma_{\text{net}}^{\text{rem}}$ as a function of $\eta = Z_p/v_p$ in the case of (a) static screening, (b) dynamical target screening, (c) dynamical target and projectile screening potentials. The systems shown are He^{2+} (---), Li^{3+} (⋯⋯), C^{6+} (—), Ne^{10+} (·-·). Adapted from [7]

surprising in the nonperturbative $\eta \geq 1$ region, but based on the present $\hbar = 0$ mean-field calculations alone we cannot draw definitive conclusions. Ultimately, experimental data would be needed for a better understanding of the strength of the high-multiplicity electron removal processes as a function of η .

C. Collisions with ammonia molecules

For the case of ammonia target molecules we focus on collisions with protons for which differential and total cross section data are available for comparison. As can be expected

for a singly-charged projectile, we found dynamical screening effects to be rather weak, and thus we discuss results obtained from the static screening model only. Net differential electron emission was measured some time ago [22], while total cross section data for single and multiple ionization events were reported more recently [23]. Comparing the latter with calculations requires some caution since the measurements are based on counts for charged fragments and do not directly correspond to the charge-state correlated cross sections for capture and ionization discussed in Sect. II B 2.

We show in Fig. 8 DDCS results for $E = 250$ keV proton impact as functions of the polar emission angle for a set of electron energies between $E_{\text{el}} = 10$ eV and $E_{\text{el}} = 500$ eV. Previous theoretical data are discussed in [10].

We have calculated both net DDCSs and DDCSs for $q = 1$ according to (11) and (9) and display them as solid and dashed lines, respectively. The former agree well with the measurements, particularly at high electron energies and backward angles. At low electron energies and forward angles our results fall short; we stop showing them when the number of recorded trajectories drops to very low values. This is a similar problem as encountered for electron emission from water molecules (cf. Sect. III A) and is most likely due to a known inherent deficiency of the $\hbar = 0$ approximation [24].

The comparison between the solid and dashed lines provides an indication of the significance of multiple ionization. The net and $q = 1$ results are of similar shape and typically differ by a factor of two, i.e., the calculations predict that double and higher multiple ionization contribute about equally to net ionization as the $q = 1$ channel. In the absence of q -specific DDCS data we can only speculate whether this is indeed the case in this system or if the result signals a deficiency of the IEM. We do note that NH_3 is an extended object with a number of relatively loosely bound electrons, i.e., multiple ionization might indeed be quite strong.

We end this section with a look at the total cross sections for net and $q = 1, 2, 3$ -fold ionization in Fig. 9. The present net results are calculated according to $\sigma_{\text{net}}^{\text{ion}} = \sigma_1^{\text{ion}} + 2\sigma_2^{\text{ion}} + 3\sigma_3^{\text{ion}}$, i.e., contributions from $q \geq 4$ events are neglected. IAM-PCM results from [27] are also included in the figure, and so are net measurements from [22] and σ_q^{ion} data from [23] obtained by summing up fragmentation yields.

The present net cross section is quite close to the data point at $E = 250$ keV, but falls below the measurements at higher energies. The calculation for $q = 1$ produces a cross section

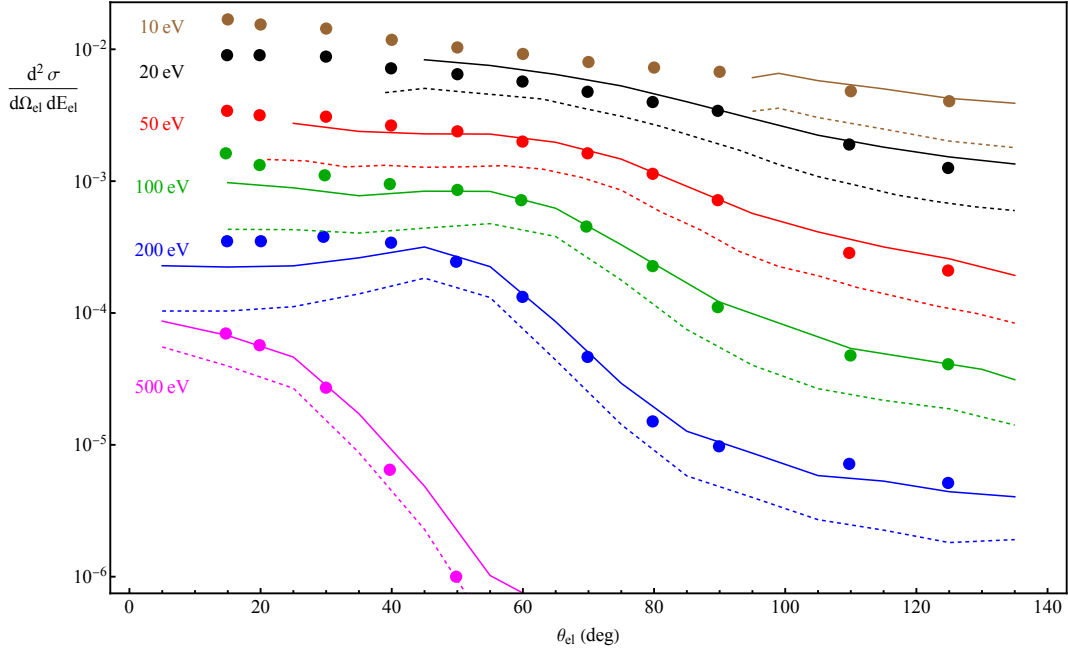


FIG. 8. DDCS in units of $\text{\AA}^2/(\text{eV srad})$ for p-NH₃ collisions at $E = 250$ keV for ionized electron energies of $E_{\text{el}} = 10, 20, 50, 100, 200, 500$ eV. Solid lines: CTMC net ionization results obtained with (11); dashed lines are for single ionization obtained with (9). The data points are the experimental results of [22], as reported in [25, 26]. At low electron emission energies and forward angles the CTMC results drop to low values and are not shown. Adapted from [10]

curve which matches the shape of the experimental data of [23] quite well, but underestimates them by about 30 %. This is different from the IAM-PCM prediction which agrees well with the $q = 1$ data at intermediate and high energies and is marginally below the two data points at $E = 125$ keV and $E = 250$ keV. Also for $q = 2$ and $q = 3$ do the two theories differ—both in shape and in magnitude.

From a comparison of the experimental net data of [22] and the $q = 1$ data of [23] one would conclude that the net cross section is almost entirely due to single ionization, and indeed the experimental $q = 2$ and $q = 3$ data included in Fig. 9 appear to confirm this. However, the fragment measurements of [23] may miss some contributing channels, since certain coincidences cannot be detected with the set-up used. This is to say that the reasons

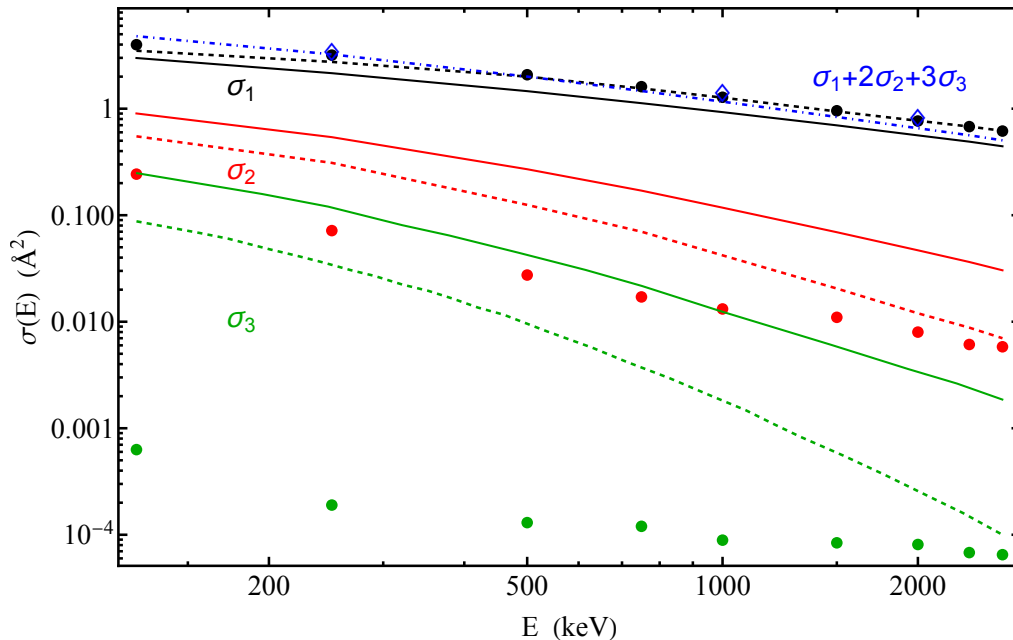


FIG. 9. Total cross sections for p-NH₃ collisions as functions of impact energy. Dash-dotted blue line: CTMC approximate net ionization result, $\sum_{q=1}^3 q\sigma_q^{\text{ion}}$. Blue open diamonds: net ionization cross sections from [22]. Solid lines (black, red, green) from top to bottom: CTMC results for σ_q^{ion} with $q = 1, 2, 3$ respectively. Dashed lines (black, red, green): IAM-PCM results shown in [23] and [27] for σ_q^{ion} . Dots (black, red, green): experimental values for σ_q^{ion} from fragmentation yields [23]. The results for $q = 3$ are associated solely with H⁺ + N²⁺ coincidences. Adapted from [10]

for the apparent very strong overestimation of double and triple ionization by the present CTMC as well as the previous IAM-PCM calculations remain somewhat unclear. We refer the reader to [10] for a more detailed discussion of this issue.

IV. CONCLUDING REMARKS

We have presented a mean-field model applied at the $\hbar = 0$ level to deal with the problem of capture and ionization in ion-molecule collisions. Both differential and total cross sections were calculated, and a select set of results for various ions impinging on water and ammonia molecules have been discussed in comparison with experimental data and some of the existing previous calculations. These comparisons shed light on the strengths and weaknesses of the model and on open questions.

To summarize our findings, we start with noting that the use of multicenter potentials to describe the molecular targets appears to be a plus compared to previous calculations in which the molecular geometry was modelled in less sophisticated fashions. This is most obvious in angular electron distributions. The comparisons provided suggest that the notion of two-center electron emission, extensively discussed for ion-atom collision problems, has to be replaced by many-center electron emission for molecular targets.

The IEM framework used includes the straightforward calculation of multiple capture and ionization contributions via multinomial statistics. We have found that contributions from multiplicities higher than $q = 1$ can be quite substantial, even for singly-charged ion impact. To which extent this reflects the physics at play or a shortcoming of the IEM remains to be seen, given that the existing coincident experiments for molecular targets are based on the counting of charged fragments and may suffer from incomplete detection, i.e., certain contributions might be missed and others misidentified. Further experimental investigation and also theoretical efforts which do not rely on the IEM are needed to shed more light on this problem.

One limitation of the present CTMC model is its inability to describe correctly the forward emission of low-energy electrons. This problem cannot be fixed easily, certainly not without going beyond the $\hbar = 0$ level of the theory. This, however, appears to be challenging to say the least, unless one is willing to compromise on other aspects of the problem at hand, such as its multicenter nature. It is thus safe to conclude that CTMC models, despite their imperfections, will continue to play an important role in aiding the understanding of ion-molecule collision problems.

ACKNOWLEDGMENTS

Financial support from the Natural Sciences and Engineering Research Council of Canada (NSERC) (RGPIN-2017-05655 and RGPIN-2019-06305) is gratefully acknowledged.

-
- [1] A. Messiah, *Quantum Mechanics I* (North Holland, Amsterdam, 1961) Chap. 6.
 - [2] R. Abrines and I. C. Percival, *Proceedings of the Physical Society* **88**, 861 (1966).

- [3] J. Ullrich, R. Moshhammer, R. Dörner, O. Jagutzki, V. Mergel, H. Schmidt-Böcking, and L. Spielberger, *Journal of Physics B: Atomic, Molecular and Optical Physics* **30**, 2917 (1997).
- [4] C. L. Cocke and R. E. Olson, *Physics Reports* **205**, 153 (1991).
- [5] F. Frémont, *Classical Treatment of Collisions Between Ions and Atoms or Molecules* (Springer Nature, Cham, 2021).
- [6] A. Jorge, M. Horbatsch, C. Illescas, and T. Kirchner, *Phys. Rev. A* **99**, 062701 (2019).
- [7] A. Jorge, M. Horbatsch, and T. Kirchner, *Phys. Rev. A* **102**, 012808 (2020).
- [8] H. J. Lüdde, A. Jorge, M. Horbatsch, and T. Kirchner, *Atoms* **8**, 59 (2020).
- [9] A. Bhogale, S. Bhattacharjee, M. R. Chowdhury, C. Bagdia, M. F. Rojas, J. M. Monti, A. Jorge, M. Horbatsch, T. Kirchner, R. D. Rivarola, and L. C. Tribedi, *Phys. Rev. A* **105**, 062822 (2022).
- [10] A. Jorge, M. Horbatsch, and T. Kirchner, “Classical-trajectory model for ionizing proton-ammonia molecule collisions: the role of multiple ionization,” (2022).
- [11] C. Illescas, L. F. Errea, L. Méndez, B. Pons, I. Rabadán, and A. Riera, *Phys. Rev. A* **83**, 052704 (2011).
- [12] R. Moccia, *The Journal of Chemical Physics* **40**, 2176 (1964).
- [13] T. Kirchner, M. Horbatsch, H. J. Lüdde, and R. M. Dreizler, *Phys. Rev. A* **62**, 042704 (2000).
- [14] M. Murakami, T. Kirchner, M. Horbatsch, and H. J. Lüdde, *Phys. Rev. A* **85**, 052704 (2012).
- [15] S. Bhattacharjee, S. Biswas, C. Bagdia, M. R. Chowdhury, S. Nandi, D. Misra, J. M. Monti, C. A. Tachino, R. D. Rivarola, C. Champion, and L. C. Tribedi, *Journal of Physics B: Atomic, Molecular and Optical Physics* **49**, 065202 (2016).
- [16] S. Bhattacharjee, S. Biswas, J. M. Monti, R. D. Rivarola, and L. C. Tribedi, *Phys. Rev. A* **96**, 052707 (2017).
- [17] S. Bhattacharjee, C. Bagdia, M. R. Chowdhury, J. M. Monti, R. D. Rivarola, and L. C. Tribedi, *The European Physical Journal D* **72**, 15 (2018).
- [18] P. D. Fainstein, V. H. Ponce, and R. D. Rivarola, *Journal of Physics B: Atomic, Molecular and Optical Physics* **24**, 3091 (1991).
- [19] N. Stolterfoht, R. D. DuBois, and R. D. Rivarola, *Electron Emission in Heavy Ion–Atom Collisions* (Springer, Berlin, 1997).
- [20] H. Luna, W. Wolff, E. C. Montenegro, A. C. Tavares, H. J. Lüdde, G. Schenk, M. Horbatsch, and T. Kirchner, *Phys. Rev. A* **93**, 052705 (2016).

- [21] H. J. Lüdde, A. Achenbach, T. Kalkbrenner, H.-C. Jankowiak, and T. Kirchner, *Eur. Phys. J. D* **70**, 82 (2016).
- [22] D. Lynch, L. Toburen, and W. Wilson, *The Journal of Chemical Physics* **64**, 2616 (1976).
- [23] W. Wolff, H. Luna, E. C. Montenegro, and L. C. Rodrigues Junior, *Phys. Rev. A* **102**, 052821 (2020).
- [24] C. O. Reinhold and J. Burgdörfer, *Journal of Physics B: Atomic, Molecular and Optical Physics* **26**, 3101 (1993).
- [25] B. Senger, *Zeitschrift für Physik D Atoms, Molecules and Clusters* **9**, 79 (1988).
- [26] A. Mondal, S. Halder, S. Mukherjee, C. R. Mandal, and M. Purkait, *Phys. Rev. A* **96**, 032710 (2017).
- [27] H. J. Lüdde, M. Horbatsch, and T. Kirchner, *Phys. Rev. A* **106**, 022813 (2022).